

GaAs-based polarization modulators for microwave photonic applications

Yu XIANG, Shilong PAN (✉)

Key Laboratory of Radar Imaging and Microwave Photonics, Ministry of Education,
Nanjing University of Aeronautics and Astronautics, Nanjing 211106, China

© Higher Education Press and Springer-Verlag Berlin Heidelberg 2016

Abstract GaAs-based polarization modulators (PolMs) exhibit the unique characteristic of simultaneous intensity and complementary phase modulation owing to the linear electro-optic (LEO) effect determined by crystallographic orientations of the device. In this paper, we reviewed the principle of operation, the design and fabrication flows of a GaAs-based PolM. Analytical models are established, from which the features of a PolM are derived and discussed in detail. The recent advances in PolM-based multifunctional systems, in particular the PolM-based optoelectronic oscillator (OEO) are demonstrated with an emphasis on the remarkable development of applications for frequency conversion, tunable microwave photonic filter (MPF), optical frequency comb (OFC), arbitrary waveform generation (AWG) and beamforming. Challenges in practical implementation of the PolM-based systems and their promising future are discussed as well.

Keywords GaAs, polarization modulator (PolM), optoelectronic oscillator (OEO), frequency conversion, microwave photonics filter (MPF)

1 Introduction

Microwave photonics (MWP) has attracted significant research efforts over the past two decades as a promising technology to pave the road to innovative and improved functions in information and communication systems by combining the microwave and photonics technologies [1–4]. Benefiting from the compact size, lightweight, low power consumption, wide bandwidth, large tunability and strong immunity to electromagnetic interference, MWP have promoted and expanded its applications in signal generation and processing in defense and network infrastructures [5–9]. As one of the key components in

MWP systems or integrated microwave photonic (IMWP) circuits, external optical modulators are implemented for electrical-to-optical (E/O) conversion by manipulating the amplitude and/or the phase of optical carrier. Compared to direct modulation of a laser source, external modulation scheme exhibits no linewidth broadening, frequency chirping and offers wider bandwidth [10–12].

Altering the applied electric field induces refractive index changes of the material as well as absorption edge shifts, and therefore the external modulators are conventionally categorized into electro-optic modulators (EOMs) [13] and electro-absorption modulators (EAMs) [14], attributed to several physical mechanisms including Pockels effect, Kerr effect, and Franz-Keldysh effect, quantum-confined Stark effect, free-carrier absorption, band-filling effect, respectively. The electro-optic effect is simply an electric field dependent refractive index change with no change of transparency at the working wavelength, which can be applied to realize an ideal phase modulator (PM) using a straight electro-optic waveguide. When built into a suitable integrated interferometer structure, e.g., the universally favored Mach-Zehnder interferometer (MZI), two such phase modulators make an ideal intensity modulator (IM). Whereas the change in the imaginary part of the refractive index (i.e., the absorption term) inevitably induces a substantial accompanying phase modulation, which results in non-ideal performance of the EAMs. Despite the EAMs have been demonstrated with a bandwidth of beyond 100 GHz [15], a low drive voltage of 0.2 V [16] and an extinction ratio of 30 dB [17], the EOMs, on the other hand, are simpler in concept, more versatile and mature without considerations such as carrier transport dynamics, heating effect, and wavelength sensitivity. Material pursuing with suitable electro-optic properties and practical fabrication requirements limit the choices to semiconductors (e.g., Si-, GaAs-, InP-based) [18–20], ferroelectric ceramics (e.g., LiNbO₃) [21] and electro-optic polymers [22].

Among different types of electro-optic materials, the

polymer-based modulators have higher electro-optic coefficients than those of LiNbO₃ and semiconductor ones. However, thermal stability issue causes reduction of the coefficients with the time. Given the low drive voltage, wideband modulation with moderate optical and insertion losses and good linearity, in particular a higher electro-optic coefficient than semiconductor modulators (e.g., at 1.5 μm, $r_{41} \approx 1.5$ pm/V for GaAs, $r_{33} \approx 30.9$ pm/V for LiNbO₃), LiNbO₃ modulators reached the commercial availability first. On the other hand, modulators based on LiNbO₃ cannot be incorporated with semiconductor integrated devices, which makes them only suited to external modulation applications until this day. With the progresses in compound material growth and CMOS compatible process technologies, GaAs became an ideal material candidate for research development of EOMs, owing to its environmental stability, low optical loss, power handling, linearity, large bandwidth, and last but not least, the potential extension in opto-electronic integrated circuits (OEICs) by monolithic integration of photonic devices and components. Compared with InP-based EOMs, GaAs is a low-cost technology, both for the raw material and the process-route. Tremendous work carried out throughout the 1980s and 1990s had made remarkable progress in the discrete device optimization concentrating on the bandwidth and drive parameters [19,23–35]. It is essential to modify the device geometry and layer configuration in order to obtain the maximum phase shift per unit length, per voltage applied. Thanks to the maturity of material epitaxy and traveling-wave (TW) technologies, the qualified GaAs-based EOM products for aerospace and telecommunication applications have been commercially available since the 1990s. In addition to the progress of GaAs-based Mach–Zehnder modulators (MZMs) [36,37], the polarization modulator (PolM) has been studied extensively, which initially was studied as a polarization converter [38–40]. The unique features of the PolM revealed by subsequent research efforts facilitate multi-function MWP modules with high flexibility compared to the conventional IM and PM.

In this paper, we perform a review of the principle of operation, the design and fabrication flows, and the MWP application of a GaAs-based PolM. The paper is organized as follows: in Section 2, physical mechanism of the PolM and its principle of operation will be reviewed, from both of the optical and electrical perspective, followed by the description of design and fabrication of such devices in Section 3. The various MWP systems based on the PolM will be introduced and analyzed in Section 4. The conclusion and discussion will be provided in Section 5.

2 Principle of GaAs-based PolMs

GaAs belongs to the $\bar{4}3m$ zincblende crystal symmetry

group and is not intrinsically birefringent. In a GaAs-based PolM, the linear electro-optic (LEO) effect is utilized to give rise to an electric-field induced birefringence. Due to the fabrication convenience, the principal x , y and z axes are defined along the $[1\ 1\ 0]$, $[-1\ 1\ 0]$ and $[0\ 0\ 1]$ directions, the waveguide fabricated on a $(0\ 0\ 1)$ substrate is along y direction with an angle φ ($\varphi = 45^\circ$) to the $[0\ 1\ 0]$ crystallographic direction. With the applied voltage, an electrical field E perpendicular to the waveguide is on the x axis, that is, $[1\ 1\ 0]$ direction. The electro-optic coefficient matrix with respect to the new xyz axes is given by

$$\begin{bmatrix} 0 & 0 & r_{41}\sin(2\varphi) \\ 0 & 0 & -r_{41}\sin(2\varphi) \\ 0 & 0 & 0 \\ r_{41}\cos(2\varphi) & -r_{41}\sin(2\varphi) & 0 \\ r_{41}\sin(2\varphi) & r_{41}\cos(2\varphi) & 0 \\ 0 & 0 & r_{41}\cos(2\varphi) \end{bmatrix}. \quad (1)$$

The index ellipsoid can be written as

$$B_{11}x^2 + B_{22}y^2 + B_{33}z^2 + 2B_{12}xy + 2B_{13}xz + 2B_{23}yz = 1. \quad (2)$$

For the light propagating in y direction, the cross-section of the index ellipsoid can be obtained by setting $y = 0$ in Eq. (2),

$$B_{11}x^2 + B_{33}z^2 + 2B_{13}xz = 1, \quad (3a)$$

where

$$\begin{cases} B_{11} = \frac{1}{n_0^2}, \\ B_{33} = \frac{1}{n_0^2}, \\ B_{13} = r_{41}\sin(2\varphi)E = r_{41}E. \end{cases} \quad (3b)$$

The major and minor axes of the ellipse described by Eq. (3a) are defined as the new axes x' and z' which have an angle θ to x and z , respectively, where θ is given by

$$\tan(2\theta) = \frac{2B_{13}}{B_{11} - B_{33}}, \quad (4)$$

since $B_{11} = B_{33}$, $\theta = 45^\circ$, and Eq. (3a) can be simplified in the $x'z'$ coordinates as

$$\frac{x'^2}{n_x^2} + \frac{z'^2}{n_z^2} = 1, \quad (5a)$$

where

$$\begin{cases} n_x = \left(\frac{1}{n_0^2} + B_{13} \right)^{-\frac{1}{2}} \approx n_0 - \frac{1}{2}n_0^3 r_{41}E, \\ n_z = \left(\frac{1}{n_0^2} - B_{13} \right)^{-\frac{1}{2}} \approx n_0 + \frac{1}{2}n_0^3 r_{41}E. \end{cases} \quad (5b)$$

When a horizontal electric field is applied along x axis, it perturbs the index ellipsoid via the electro-optic effect. The principal axes of the intersection index ellipse are in the xz plane with a fixed $\theta = 45^\circ$ with respect to the electrical field components of the transverse electric (TE) and transverse magnetic (TM) eigenmodes of the optical waveguide, independent of the electric field E , as shown in Fig. 1. Moreover, the changes in the optical indicatrix along the fast and slow axes are of the exact same value, which depends on the electric field E , but with opposite signs. The incident TE-like polarization mode, which is parallel to the x axis, could be resolved into components on the fast and slow axes. As a result of the refractive index difference, the TE (TM)-like incident polarization mode will convert to the orthogonal linear polarization, which is TM (TE)-like mode, passing through elliptical and circular polarization states as along the great longitudinal circle on the Poincaré sphere. The energy transfer between the TE and TM modes is the basis of the operation of the GaAs-based mode converters.

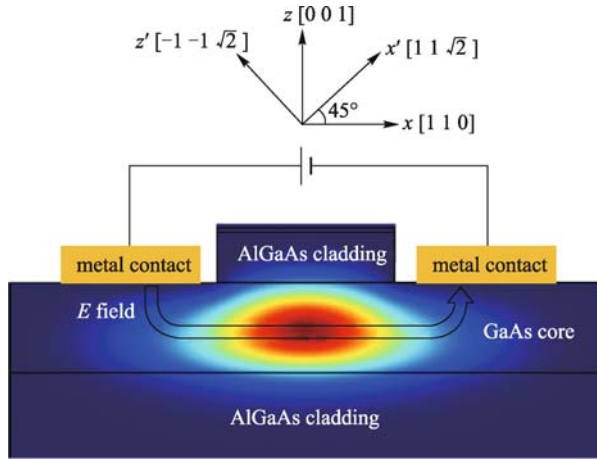


Fig. 1 Calculated cross-sectional intensity of fundamental TE mode at $1.5 \mu\text{m}$ confined in the GaAs layer

The index ellipsoid perturbation results in the coupling of the TE and TM modes in the unperturbed waveguide attributing to the presence of the off-axis index ellipsoid components. According to the coupled mode theory [41], the perturbations to the TE and TM propagation constants can be described as

$$\begin{cases} n_{\text{TE,TM}} = \frac{\beta_{\text{TE,TM}}\lambda_0}{2\pi}, \\ \Delta\beta_{\text{TE}} = \sqrt{\delta^2 + \kappa^2} - \delta, \\ \Delta\beta_{\text{TM}} = -(\sqrt{\delta^2 + \kappa^2} - \delta), \\ \delta = \frac{\beta_{\text{TE}} - \beta_{\text{TM}}}{2}, \\ \kappa = \frac{\pi n_0^3 r_{41} E}{\lambda_0}, \end{cases} \quad (6)$$

where κ is the coupling constant, λ_0 is the free-space optical wavelength, β_{TE} and β_{TM} are the unperturbed propagation constants. The equation above indicates that the magnitude of the propagation constant perturbation is the same with different signs for the TE and TM modes respectively, which can be controlled by the applied voltage. Therefore, the device can be used as a PolM with opposite modulation indices of the two modes, with a static phase shift determined by the DC bias as expressed by the Jones matrix

$$\mathbf{J} = \begin{bmatrix} \exp\left(j\frac{\gamma\phi(t)}{2} + j\frac{\phi_0}{2}\right) & 0 \\ 0 & \exp\left(-j\frac{\gamma\phi(t)}{2} - j\frac{\phi_0}{2}\right) \end{bmatrix}, \quad (7)$$

where γ is the phase modulation index, ϕ_0 is the static phase shift and $\phi(t)$ is the modulating signal.

3 Design and fabrication of GaAs-based PolMs

In a rib waveguide consisting of typical graded-index $\text{Al}_x\text{Ga}_{1-x}\text{As}$ compound materials for guided modes at $\lambda_0 = 1.3$ or $1.55 \mu\text{m}$, the effective index n_{eff} is about 3.2 to 3.4. The microwave index, n_m for a typical surface-deposited coplanar strips (CPS) on a GaAs substrate can be approximated by

$$n_\mu = \sqrt{\frac{\varepsilon_r + 1}{2}}, \quad (8)$$

where ε_r is the dielectric constant of the GaAs, which results in a $n_\mu \approx 2.6$. As denoted in previous section, the waveguide and E are along the y and x axes respectively, therefore, the TW electrodes are along the y direction. Assuming the beginning position of the electrode located at $y = 0$, the voltage “seen” by an incident optical wave can be expressed as

$$V(y,t) = V_b + V_0 e^{-\alpha y} \cos\left(\frac{2\pi f_\mu}{c}(n_\mu - n_{\text{eff}})y - 2\pi f_\mu t\right), \quad (9)$$

where V_b is the DC bias, α is the microwave loss in the unit of cm^{-1} , and f_μ is the microwave frequency. To achieve high modulation bandwidth, great attention has to be paid to avoid the reflection of microwave signal in transmission line and walk-off between the microwave and optical wave by ensuring an electrode with characteristic impedance of $Z_0 \approx 50 \Omega$, equalizing the indices of n_{TE} , n_{TM} and n_μ , as well as to minimize the loss α . The designated line capacitance C and inductance per unit length L of the TW electrode can be calculated according to

$$\begin{cases} n_{\mu} = c\sqrt{LC}, \\ Z_0 = \sqrt{\frac{L}{C}}. \end{cases} \quad (10)$$

The slow-wave electrodes is one of the most critical challenges for designs of GaAs-based modulators, including the PolMs [31–34]. A typical layout of such slow-wave CPS electrode employs periodically loaded capacitive elements consisting of fins and pads, which is illustrated in Fig. 2. The geometry of these fins and pads are supposed to be smaller enough than microwave wavelength so as to behave like equipotential surfaces, resulting in a higher value of n_{μ} due to an increased C together with a slightly decreased L . By tuning the dimensions of the slow-wave electrode, not only the velocity match and 50 Ω characteristic impedance could be obtained simultaneously, a narrow gap between the pads with remotely located main electrodes would also allow for a high E and a low α .

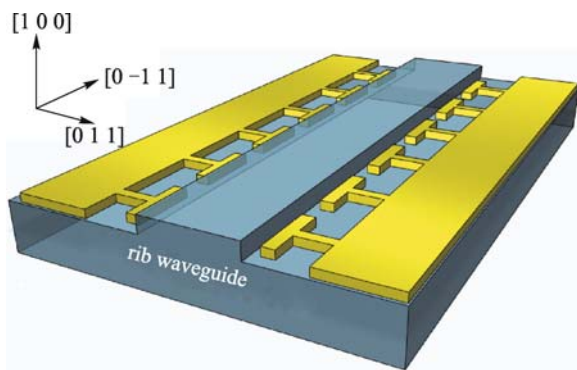


Fig. 2 Schematic of a PolM with slow-wave, CPS, TW electrodes

The fabrication sequence of a GaAs-based PolM begins with the molecular beam epitaxy (MBE) or metal-organic chemical vapor deposition (MOCVD) of the layer stack on a (100) semi-insulating (SI) GaAs substrate. The layer configuration is demonstrated in Fig. 3(a), which consists of a GaAs core layer sandwiched between two $\text{Al}_x\text{Ga}_{1-x}\text{As}$ cladding layers, and a GaAs cap layer on top for passivation. In case of surface defects, a GaAs buffer layer is also necessary between the SI substrate and the $\text{Al}_x\text{Ga}_{1-x}\text{As}$ cladding layer. To ensure a low microwave loss, researchers pointed out that the unintentional doping level in the epitaxial layer structures has to be under the control of lower than 10^{14} cm^{-3} [42]. The process flow of the device is depicted in Figs. 3(b) and 3(c), the optical rib waveguide definition and the TW electrodes deposition are implemented by means of dry etching and lift-off process respectively.

The microwave measurement of fabricated TW electrodes is of great concern since the S-parameters can be used

to derive Z_0 , α and n_{μ} at high frequency modulation via the following equations [43,44].

$$\begin{cases} Z_0 = 50 \frac{(1 + s_{11})(1 + s_{22}) - s_{12}s_{21}}{s_{22} - s_{11} \pm \sqrt{(1 + s_{12}s_{21} - s_{11}s_{22})^2 - 4s_{21}}}, \\ \alpha + j \frac{2\pi f_{\mu} n_{\mu}}{c} = \frac{1}{l} \ln \left[\frac{1 + s_{12}s_{21} - s_{11}s_{22}}{2s_{21}} \right. \\ \left. \pm \sqrt{\left(\frac{1 + s_{12}s_{21} - s_{11}s_{22}}{2s_{21}} \right)^2 - 1} \right], \end{cases} \quad (11)$$

where l is the electrode length. The solutions in the equations above are chosen so that the real part of Z_0 and value of α are positive.

4 Analytical models and features of MWP systems based on PolMs

Superior to the IMs and PMs which have been playing the very important role of E/O conversion in all MWP systems, GaAs-based PolMs offer two-dimensional modulation instead of one (either intensity or phase) by supporting simultaneous modulation of TE and TM modes with opposite phase modulation indices. In the company of polarization controllers (PCs), polarization beam splitters (PBSs) and optical filters, more and more elegant and innovative MWP systems have been implemented, covering the applications of signal generation and processing.

4.1 Signal generation

The generation of high quality microwave signals with spectral purity, frequency stability and low phase noise has always been a hot topic of MWP. In 1994, Yao and Maleki from Jet Propulsion proposed an OEO employing an EOM, a photodetector (PD), an amplifier and an electrical bandpass filter (BPF) to achieve oscillation up to 75 GHz [45]. By converting the oscillating signal from electrical domain to optical domain, the high- Q optical energy storage components, wideband photonic devices and processing techniques facilitate high frequency microwave signals with low phase noise. In reality, however, this approach may suffer from the bias drifting problem of the MZM, which results in the stability issue unless a sophisticated control circuit is applied, as well as the difficulty in maintaining an ideal 50/50 splitting ratio in a Y-splitter due to fabrication tolerances. By replacing the MZM with a GaAs-based PolM incorporated with a PC and a polarizer, an OEO enabling the generation of fundamental frequency, frequency-doubling, frequency-quadrupling and frequency-sextupling signals can be

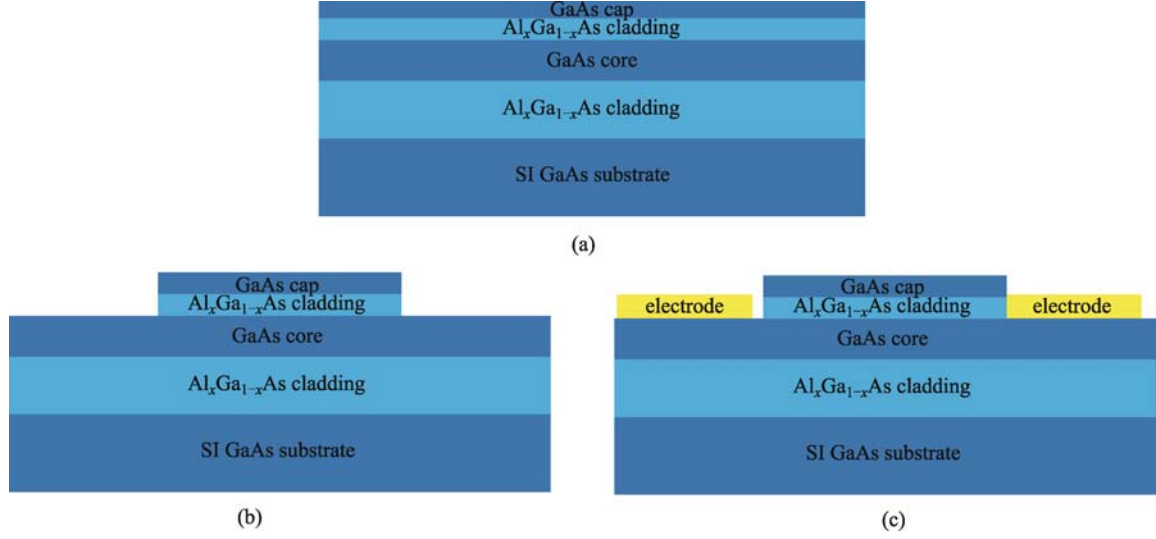


Fig. 3 (a) Layer configuration of a typical GaAs-based PolM; (b) definition of the rib waveguide by dry etching; (c) deposition of the metal electrodes by a standard lift-off process

obtained without the drifting problem.

According to Eq. (7), a linear-polarized light E_{in} throughout a PC, with an angle of 45° to one of the principal axes of the PolM is introduced to the PolM, which is followed by a polarizer aligned to have an angle of θ to one of the principal axes, the output signal is simply the interference of the two polarization mode components along the polarizer direction,

$$E_{out} = \frac{\sqrt{2}}{2} E_{in} \left\{ \cos\theta \exp \left[j \left(\frac{\gamma\phi(t)}{2} + \frac{\phi_0}{2} \right) \right] + \sin\theta \exp \left[-j \left(\frac{\gamma\phi(t)}{2} + \frac{\phi_0}{2} \right) \right] \right\}. \quad (12)$$

As can be seen from the equation above, when θ is 0° or 90° , the phase modulation with either positive or negative modulation index is obtained, and when θ is 45° ,

$$E_{out} = E_{in} \cos \left(\frac{\gamma\phi(t) + \phi_0}{2} \right), \quad (13)$$

which represents a typical intensity modulation, and as a matter of fact, is equivalent to the output of a MZM. Therefore, the biasing points in a MZM at the maximum transmission point (MATP), quadrature point (QTP) and the minimum transmission point (MITP) are corresponding to the static phase shift $\phi_0 = 0, \pi/2$ and π , respectively. For θ of other values, Eq. (12) is rewritten as (14), the incident signal will be phase- and intensity-modulated simultaneously, which is equivalent to an intensity modulation with tunable chirp, and the chirp coefficient can be adjusted by tuning the angle θ .

$$E_{out} = \frac{\sqrt{2}}{2} E_{in} \left\{ 2\cos\theta \cos \left(\frac{\gamma\phi(t)}{2} + \frac{\phi_0}{2} \right) \right.$$

$$\left. + (\sin\theta - \cos\theta) \exp \left[-j \left(\frac{\gamma\phi(t)}{2} + \frac{\phi_0}{2} \right) \right] \right\}. \quad (14)$$

The mixed modulation provides a new solution to compensate the dispersion-induced power fading and intermodulation distortion in analog photonic link [46]. Besides, when the chirp interacts with fiber dispersion, a frequency-tunable microwave photonic filter (MPF) can be achieved, which will be explained in detail in the next section.

Assuming a single-frequency modulation signal, i.e., $\phi(t) = \cos(\omega_m t)$, the output signal of Eq. (13) can be expressed as

$$E_{out} = E_{in} \left\{ \cos \left(\frac{\phi_0}{2} \right) J_0(\gamma) + 2\cos \left(\frac{\phi_0}{2} \right) \sum_{n=1}^{\infty} J_{2n}(\gamma) (-1)^n \cos(2n\omega_m t) + 2\sin \left(\frac{\phi_0}{2} \right) \sum_{n=1}^{\infty} J_{2n-1}(\gamma) (-1)^n \cos((2n-1)\omega_m t) \right\} \quad (15)$$

based on the Jacobi-Anger expansion, where J_n is the n th-order Bessel function of the first kind. When $\phi_0 = \pi$, the equation above becomes

$$E_{out} = 2E_{in} \sum_{n=1}^{\infty} J_{2n-1}(\gamma) (-1)^n \cos((2n-1)\omega_m t). \quad (16)$$

Only odd-order sidebands are left, to be specific, only the ± 1 st-order sidebands are left in the case of small signal modulation. As a result, a frequency-doubled microwave signal can be obtained by beating the two 1st-order

sidebands at a PD [47], which generates an electrical signal as

$$I(t) \propto A\mathfrak{R}J_1^2(\gamma)\cos(2\omega_m t), \quad (17)$$

where \mathfrak{R} is the responsivity of the PD, and A is a parameter related to the input optical power. In the case of large signal modulation, the 3rd-order sidebands in Eq. (16) shall not be ignored. The frequency-sextupled microwave signal can be generated by filtering out the optical carrier, two 1st-order sidebands and beating the 3rd-order sidebands at a PD [48]. The frequency-sextupled microwave signal can be expressed in the way analogous to Eq. (17), as

$$I(t) \propto A\mathfrak{R}J_3^2(\gamma)\cos(6\omega_m t). \quad (18)$$

When $\phi_0 = 0$, only the even-order sidebands are left and output signal at the polarizer becomes

$$E_{\text{out}} = E_{\text{in}} \left(J_0(\gamma) + 2 \sum_{n=1}^{\infty} J_{2n}(\gamma) (-1)^n \cos(2n\omega_m t) \right). \quad (19)$$

Under small signal modulation, the frequency-quadrupled microwave signal can be obtained by filtering out the optical carrier and beating the two 2nd-order sidebands at a PD,

$$I(t) \propto A\mathfrak{R}J_2^2(\gamma)\cos(4\omega_m t). \quad (20)$$

As discussed above, the PolM-based OEO is a promising approach to generate low phase noise, high-frequency electrical local oscillator (LO) signal using low-frequency devices and a wideband PD. Owing to the PC and polarizer as external elements to the PolM, both the angle θ between the polarization direction of the polarizer

and the principal axes of the PolM, and the static phase difference ϕ_0 can be adjusted. As a result, the PolM not only become DC bias free, but also enable multichannel operation, serving as a LO and frequency upconversion simultaneously [49,50], as shown in Fig. 4. In addition, frequency downconversion is achievable as well by a PolM-based OEO [51], which has been successfully applied in a radio-over-fiber (ROF) link for the wireless distribution of a 3 Gb/s uncompressed HD video [52].

Another important signal generation application of the PolM-based OEO is the arbitrary waveform generation (AWG). One of the novel schemes is to generate a frequency-hopping microwave waveform by means of a wideband frequency-tunable bandpass MPF incorporated in an OEO loop, which consists of a PolM followed by a polarization-maintaining phase-shifted fiber Bragg grating (PM-PSFBG) [53]. The frequency response profile of the overall MPF, in particular, the oscillation frequency depends on the state of polarization (SOP) of the light wave at the output of PolM. Therefore, as the control signal applied to the PolM manipulating the SOP of the light wave, the oscillation frequency alters correspondingly and gives rise to high-speed frequency hopping. Alternatively, the optical frequency comb (OFC) leads to the implementation of the AWG [54]. A number of approaches based on the PolMs have been proposed to generate OFCs, such as using a single PolM [55], a single PolM with the assistance of a Brillouin-assisted power equalizer [56], two cascaded PolMs [57], and two cascaded PolMs with an OEO scheme [58].

4.2 Signal processing

In the MWP signal processing, MPF is one of the most

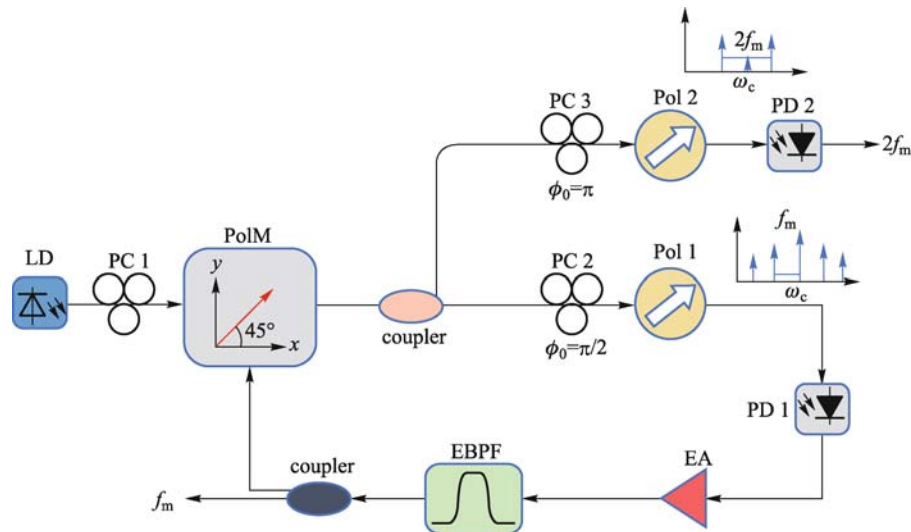


Fig. 4 Schematic of a PolM-based frequency-doubling OEO. LD: laser diode, PC: polarization controller, PolM: polarization modulator, PD: photodiode, EA: electric amplifier, EBPF: electric bandpass filter

important application. As pointed out at the end of previous section, a PolM in conjunction with a dispersive element, e.g., a chirped fiber Bragg grating (CFBG), performs as a wideband frequency-tunable MPF with the peak of the frequency response controlled by simply tuning the PC [59]. Stemming from Eq. (12) and assuming the case of small signal modulation, the signal at the output of dispersive element becomes

$$\begin{aligned}
 E_{\text{out}} = & \frac{\sqrt{2}}{2} E_{\text{in}} \left\{ J_0\left(\frac{\gamma}{2}\right) \left\{ \cos\theta \exp \left[j\left(\frac{\phi_0}{2} + \theta_0\right) \right] \right. \right. \\
 & \left. \left. + \sin\theta \exp \left[j\left(-\frac{\phi_0}{2} + \theta_0\right) \right] \right\} \right. \\
 & \left. + J_1\left(\frac{\gamma}{2}\right) \cos\theta \left\{ \exp \left[j\left(\omega_m t + \frac{\pi}{2} + \frac{\phi_0}{2} + \theta_{+1}\right) \right] \right. \right. \\
 & \left. \left. - \exp \left[j\left(-\omega_m t - \frac{\pi}{2} + \frac{\phi_0}{2} + \theta_{-1}\right) \right] \right\} \right. \\
 & \left. + J_1\left(\frac{\gamma}{2}\right) \sin\theta \left\{ \exp \left[j\left(\omega_m t + \frac{3\pi}{2} - \frac{\phi_0}{2} + \theta_{+1}\right) \right] \right. \right. \\
 & \left. \left. - \exp \left[j\left(-\omega_m t - \frac{3\pi}{2} - \frac{\phi_0}{2} + \theta_{-1}\right) \right] \right\} \right\}, \quad (21)
 \end{aligned}$$

where θ_0 , θ_{+1} and θ_{-1} , are the dispersion-induced phase shifts to the optical carrier, the upper 1st-order sideband and the lower 1st-order sideband, respectively. Expanding the propagation constant in the Taylor series, the dispersion induced phase shifts becomes

$$\begin{cases} \theta_0 = z\beta(\omega_c), \\ \theta_{-1} = z\beta(\omega_c) - \tau_0\omega_m + \frac{1}{2}D_\omega\omega_m^2, \\ \theta_{+1} = z\beta(\omega_c) + \tau_0\omega_m + \frac{1}{2}D_\omega\omega_m^2, \end{cases} \quad (22)$$

where ω_c is the angular frequency of the optical carrier, z is the transmission distance, τ_0 equals to $z\beta'(\omega_c)$, D_ω equals to $z\beta''(\omega_c)$, and β' and β'' are the first- and second-order derivatives of the propagation constant with respect to ω_c . Beating the optical signal at a PD and setting the phase difference ϕ_0 to be $\pi/2$, the AC current is given by

$$I(t) \propto 2J_0\left(\frac{\gamma}{2}\right)J_1\left(\frac{\gamma}{2}\right)\sin\left(2\theta + \frac{1}{2}D_\omega\omega_m^2\right)\cos[\omega_m(t - \tau_0)]. \quad (23)$$

The transmission response of this frequency-tunable MPF is

$$|h(\omega_m)| \propto \left| 2J_0\left(\frac{\gamma}{2}\right)J_1\left(\frac{\gamma}{2}\right)\sin\left(2\theta + \frac{1}{2}D_\omega\omega_m^2\right) \right|. \quad (24)$$

As Eq. (24) reveals, the transfer function has a periodic

behavior and the center frequencies at the maximum transmittance are at

$$\begin{aligned}
 \omega_{m,\text{peak}} = & \sqrt{\left((2k+1)\pi - 4\theta\right)/D_\omega}, \\
 & k = 0, \pm 1, \pm 2, \dots \quad (25)
 \end{aligned}$$

The center frequencies of the MPF allow for tuning to any desired value simply by altering the angle θ via adjusting the PC between the PolM and the polarizer. Experimental result has demonstrated a tunable frequency within 5.8 to 11.8 GHz based on the proposed tunable OEO. The single-sideband (SSB) phase noise of the high-purity microwave signal was -104.56 dBc/Hz at 10-kHz offset [59].

Replacing the dispersive element with an optical bandpass filter (OBPF), a PolM-based tunable two-tap MPF with a complex coefficient enables a full tuning of the free spectral range (FSR) without any change of its shape [60]. Hence, the dispersion-induced phase shifts in Eq. (21) can be removed and what left is

$$\begin{aligned}
 E_{\text{out}} = & \frac{\sqrt{2}}{2} E_{\text{in}} \left\{ \cos\theta \exp j\left(\frac{\phi_0}{2}\right) \left[J_0\left(\frac{\gamma}{2}\right) \right. \right. \\
 & \left. \left. + jJ_1\left(\frac{\gamma}{2}\right) \exp(j\omega_m t) - jJ_{-1}\left(\frac{\gamma}{2}\right) \exp(-j\omega_m t) \right] \right. \\
 & \left. + \sin\theta \exp j\left(-\frac{\phi_0}{2}\right) \left[J_0\left(\frac{\gamma}{2}\right) - jJ_1\left(\frac{\gamma}{2}\right) \exp(j\omega_m t) \right. \right. \\
 & \left. \left. + jJ_{-1}\left(\frac{\gamma}{2}\right) \exp(-j\omega_m t) \right] \right\}. \quad (26)
 \end{aligned}$$

Assuming the upper 1st-order sidebands of both polarization modes are removed by the followed OBPF, two optical SSB signals with a phase difference of π is obtained

$$\begin{aligned}
 E_{\text{out}} = & \frac{\sqrt{2}}{2} E_{\text{in}} \left\{ \cos\theta \exp j\left(\frac{\phi_0}{2}\right) \left[J_0\left(\frac{\gamma}{2}\right) \right. \right. \\
 & \left. \left. + J_{-1}\left(\frac{\gamma}{2}\right) \exp\left(-j\omega_m t - \frac{\pi}{2}\right) \right] + \sin\theta \exp j\left(-\frac{\phi_0}{2}\right) \right. \\
 & \left. \left[J_0\left(\frac{\gamma}{2}\right) + J_{-1}\left(\frac{\gamma}{2}\right) \exp\left(-j\omega_m t + \frac{\pi}{2}\right) \right] \right\}. \quad (27)
 \end{aligned}$$

Adjusting ϕ_0 to be $\pi/2$ and sending this combined signal to a PD, the output current can be written as

$$I(t) \propto \cos\left(\omega_m t + 2\theta + \frac{\pi}{2}\right) J_0\left(\frac{\gamma}{2}\right) J_{-1}\left(\frac{\gamma}{2}\right). \quad (28)$$

Apparently, the proposed tunable MPF performance attributes to a PolM-based phase shifter. Owing to the easy control of θ via a PC, the phase of the electrical signal

would be shifted within 2π when θ is varied from 0 to π , which facilitates the frequency tunability of full range of FSR. Flat phase response over the range of 10 to 40 GHz of such a phase shifter has been achieved. Power fluctuation was typically below 0.5 dB throughout the 2π phase shift at a certain frequency. By adjusting the phase shifter, the notch center of the tunable MPF was able to be shifted over the entire FSR of 134 MHz, with a rejection ratio of more than 48 dB [60].

Since the phase shift is achieved by adjusting a PC, which is an external element to a PolM, a number of such phase shifters controlled by different PCs can be obtained sharing one laser source, one OBPF and a single PolM via an optical coupler. Intuitively, this flexible phase shifter array can be implemented to function as a simple and compact optically-controlled phased array antenna by carefully adjusting the PC in each path, which is demonstrated in Fig. 5 [61].

5 Conclusions and discussion

In this paper, the principle of operation of a GaAs-based PolM has been reviewed. The crystallographic characteristics of GaAs gives rise to an electro-optic effect that exhibits complementary phase modulation indices with respect to TE and TM modes. Special attention shall be paid to the PolM design, in particular the TW electrodes, so as to achieve modulation bandwidth exceeding tens of GHz. In combination with a PC as well as either a polarizer or a PBS, a GaAs-based PolM performs simultaneous modulation of the phase and intensity in optical domain. The mixed modulation can be used to reduce the dispersion-induced power fading and intermodulation distortion. The flexibility and simplicity of such two-dimension modulation offered by external elements, e.g., a PC, not only allows for a complete replacement of conventional IMs and PMs, but also enables exploration of new applications.

Analytical models revealed the working conditions under which the fundamental frequency, frequency-doubling, frequency-quadrupling and frequency-sextupling intensity modulations can be achieved mainly by a PolM. These functions can be switched in the same scheme simply by adjusting the PC between PolM and polarizer or the DC bias of the PolM. Given the unique feature of generating a low phase noise microwave signal by an OEO, the PolM-based frequency-multiplying OEO has been demonstrated to perform multichannel frequency upconversion, which is able to maintain the oscillation of the fundamental frequency in the loop while splitting it into several channels for frequency multiplying. The frequency-multiplying OEO can be used to generate microwave or millimeter-wave signals with low phase noise for applications in radars, wireless and optical communications. In addition to the photonic frequency upconversion, various schemes involving PolMs have been developed for frequency downconversion and applications of the OFC and AWG.

Inserting dispersive element between the PolM and the PC, a tunable MPF can be realized allowing for fine tuning of the oscillating frequency in an OEO with a simple control of adjusting the PC. Moreover, a continuously tunable MPF with complex coefficient exhibits tunability of the full FSR, taking advantage of the phase shifter composed of a PolM and an optical filter to perform the optical SSB modulation. Besides, the phase shifter has been implemented to the development of optical beamforming network for the application of phased array antenna.

In spite of its simplicity and flexibility in use as well as versatility in functionality, the PolM-based MWP systems require precise polarization manipulation. The performance accuracy and stability would vary as function of misalignment of the PC and environmental vibration of the system. It should be noted that the integration of GaAs-based PolMs with other key components such as waveguides structures, PCs, splitters, and couplers would

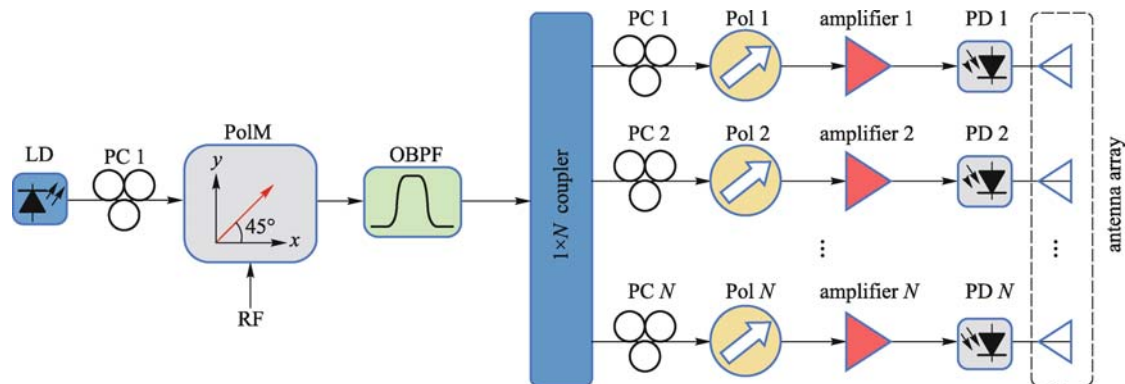


Fig. 5 Schematic of the proposed phased array antenna, in which the optical beamforming network is based on the phase shifter [61]. LD: laser diode, PC: polarization controller, PolM: polarization modulator, OBPF: optical bandpass filter, PD: photodetector

overcome the issues mentioned above. Furthermore, the significantly reduced size and improved stability of integrated microwave photonics systems would promote their practical applications extensively. The photonic integration technology on GaAs-based materials will drive the PolM-based MWP systems toward large-scale monolithic integration.

Acknowledgements This work was supported in part by the National Basic Research Program of China (No. 2012CB315705), the National Natural Science Foundation of China (Grant Nos. 61422108 and 61527820), Fundamental Research Funds for the Central Universities (Nos. NP2015404, NE2012002); and a Project Funded by the Priority Academic Program Development of Jiangsu Higher Education Institutions.

References

1. Seeds A J. Microwave photonics. *IEEE Transactions on Microwave Theory and Techniques*, 2002, 50(3): 877–887
2. Capmany J, Novak D. Microwave photonics combines two worlds. *Nature Photonics*, 2007, 1(6): 319–330
3. Yao J. Microwave Photonics. *Journal of Lightwave Technology*, 2009, 27(3): 314–335
4. Capmany J, Li G, Lim C, Yao J. Microwave photonics: current challenges towards widespread application. *Optics Express*, 2013, 21(19): 22862–22867
5. Yao J. Photonic generation of microwave arbitrary waveforms. *Optics Communications*, 2011, 284(15): 3723–3736
6. Capmany J, Mora J, Gasulla I, Sancho J, Lloret J, Sales S. Microwave photonic signal processing. *Journal of Lightwave Technology*, 2013, 31(4): 571–586
7. Pan S, Zhu D, Zhang F Z. Microwave photonics for modern Radar systems. *Transactions of Nanjing University of Aeronautics and Astronautics*, 2014, 31(3): 219–240
8. Sotom M, Benazet B, Kerrec A L, Maignan M. Microwave photonic technologies for flexible satellite telecom payloads. In: *Proceedings of 35th European Conference on Optical Communication*, Vienna, IEEE, 2009, 1–4
9. Koonen A M J, Larrode M G, Ng'oma A, Wang K, Yang H, Zheng Y, Tangdionga E. Perspectives of Radio over fiber technologies. In: *Proceedings of Optical Fiber Communication Conference*, San Diego, IEEE, 2008, 1–3
10. Yamada M, Haraguchi Y. Linewidth broadening of SCH quantum-well lasers enhanced by carrier fluctuation in optical guiding layer. *IEEE Journal of Quantum Electronics*, 1987, 23(6): 1054–1058
11. Olsen C M, Izadpanah H, Lin C. Wavelength chirp in a high- κL quarter-wave-shifted DFB laser: characterization and influence on system performance. *Journal of Lightwave Technology*, 1990, 8(12): 1810–1815
12. Jungerman R L, Johnsen C, McQuate D J, Salomaa K, Zurakowski M P, Bray R C, Conrad G, Cropper D, Hernday P. High-speed optical modulator for application in instrumentation. *Journal of Lightwave Technology*, 1990, 8(9): 1363–1370
13. Wang S Y, Lin S H. High speed III–V electrooptic waveguide modulators at $\lambda = 1.3 \mu\text{m}$. *Journal of Lightwave Technology*, 1988, 6(6): 758–771
14. Wood T H. Multiple quantum well (MQW) waveguide modulators. *Journal of Lightwave Technology*, 1988, 6(6): 743–757
15. Chaciński M, Westergren U, Stoltz B, Thylén L, Schatz R, Hammerfeldt S. Monolithically Integrated 100 GHz DFB-TWEAM. *Journal of Lightwave Technology*, 2009, 27(16): 3410–3415
16. Ueda Y, Fujisawa T, Kanazawa S, Kobayashi W, Takahata K, Ishii H. Very-low-voltage operation of Mach-Zehnder interferometer-type electroabsorption modulator using asymmetric couplers. *Optics Express*, 2014, 22(12): 14610–14616
17. Wu T H, Chiu Y J, Lin F Z. High-speed (60 GHz) and low-voltage-driving electroabsorption modulator using two-consecutive-steps selective-undercut-wet-etching waveguide. *IEEE Photonics Technology Letters*, 2008, 20(14): 1261–1263
18. Liu A, Liao L, Rubin D, Nguyen H, Ciftcioglu B, Chetrit Y, Izhaky N, Paniccia M. High-speed optical modulation based on carrier depletion in a silicon waveguide. *Optics Express*, 2007, 15(2): 660–668
19. Spickermann R, Sakamoto S R, Peters M G, Dagli N. GaAs/AlGaAs travelling wave electro-optic modulator with an electrical bandwidth > 40 GHz. *Electronics Letters*, 1996, 32(12): 1095–1096
20. Koren U, Koch T L, Presting H, Miller B I. InGaAs/InP multiple quantum well waveguide phase modulator. *Applied Physics Letters*, 1987, 50(7): 368–370
21. Noguchi K, Mitomi O, Miyazawa H. Millimeter-wave Ti:LiNbO₃ optical modulators. *Journal of Lightwave Technology*, 1998, 16(4): 615–619
22. Lee M, Katz H E, Erben C, Gill D M, Gopalan P, Heber J D, McGee D J. Broadband modulation of light by using an electro-optic polymer. *Science*, 2002, 298(5597): 1401–1403
23. Walker R G. High speed electrooptic modulation in GaAs/GaAlAs waveguide devices. *Journal of Lightwave Technology*, 1987, 5(10): 1444–1453
24. Walker R G. Broadband (6 GHz) GaAs/AlGaAs electro-optic modulator with low drive power. *Applied Physics Letters*, 1989, 54(17): 1613–1615
25. Walker R G, Bennion I, Carter A C. Low-voltage, 50 Ω , GaAs/AlGaAs travelling-wave modulator with bandwidth exceeding 25 GHz. *Electronics Letters*, 1989, 25(23): 1549–1550
26. Walker R G. High-speed III–V semiconductor intensity modulators. *IEEE Journal of Quantum Electronics*, 1991, 27(3): 654–667
27. Lin S H, Wang S Y, Hough Y M. GaAs pin electro-optic travelling-wave modulator at 1.3 μm . *Electronics Letters*, 1986, 22(18): 934–935
28. Wang S Y, Lin S H, Hough Y M. GaAs travelling-wave polarization electro-optic waveguide modulator with bandwidth in excess of 20 GHz at 1.3 μm . *Applied Physics Letters*, 1987, 51(2): 83–85
29. Kim I, Tan M R T, Wang S Y. Analysis of a new microwave low-loss and velocity-matched III–V transmission line for travelling-wave electrooptic modulators. *Journal of Lightwave Technology*, 1990, 8(5): 728–738
30. Nees J, Williamson S, Mourou G. 100 GHz travelling-wave electro-optic phase modulator. *Applied Physics Letters*, 1989, 54(20): 1962–1964
31. Jaeger N A F, Lee Z K F. Slow-wave electrode for use in compound semiconductor electrooptic modulators. *IEEE Journal of Quantum*

- Electronics, 1992, 28(8): 1778–1784
32. Jaeger N A F, Rahmatian F, Kato H, James R, Berolo E, Lee Z K F. Velocity-matched electrodes for compound semiconductor traveling-wave electrooptic modulators: experimental results. *IEEE Microwave and Guided Wave Letters*, 1996, 6(2): 82–84
 33. Spickermann R, Dagli N. Millimeter wave coplanar slow wave structure on GaAs suitable for use in electro-optic modulators. *Electronics Letters*, 1993, 29(9): 774–775
 34. Sakamoto S R, Spickermann R, Dagli N. Narrow gap coplanar slow wave electrode for travelling wave electro-optic modulators. *Electronics Letters*, 1995, 31(14): 1183–1185
 35. Spickermann R, Peters M G, Dagli N. A polarization independent GaAs-AlGaAs electrooptic modulator. *IEEE Journal of Quantum Electronics*, 1996, 32(5): 764–769
 36. Shin J H, Wu S, Dagli N. Bulk undoped GaAs–AlGaAs substrate-removed electrooptic modulators with 3.7-V-cm drive voltage at 1.55 μm . *IEEE Photonics Technology Letters*, 2006, 18(21): 2251–2253
 37. Shin J H, Chang Y C, Dagli N. 0.3 V drive voltage GaAs/AlGaAs substrate removed Mach-Zehnder intensity modulators. *Applied Physics Letters*, 2008, 92(20): 201103
 38. Rahmatian F, Jaeger N A F, James R, Berolo E. An ultrahigh-speed AlGaAs–GaAs polarization converter using slow-wave coplanar electrodes. *IEEE Photonics Technology Letters*, 1998, 10(5): 675–677
 39. Grossard N, Forte H, Vilcot J P, Beche B, Goedgebuer J P. AlGaAs–GaAs polarization converter with electrooptic phase mismatch control. *IEEE Photonics Technology Letters*, 2001, 13(8): 830–832
 40. Bull J D, Jaeger N A F, Kato H, Fairburn M, Reid A, Ghanipour P. 40 GHz electro-optic polarization modulator for fiber optic communications systems. *Proceedings of the Society for Photo-Instrumentation Engineers*, 2004, 5577: 133–143
 41. Yariv A. *Introduction to Optical Electronics*. 2nd ed. New York: Holt, Rinehart, and Winston, 1976
 42. Khazaei H R, Berolo O, James R, Wang W J, Maigné P, Young M, Ozard K, Reeves M, Ghannouchi F M. Charge carrier effect on the microwave losses observed on traveling-wave electrodes used in electro-optic modulators. *Microwave and Optical Technology Letters*, 1998, 17(4): 236–241
 43. Kiziloglu K, Dagli N, Matthaai G L, Long S I. Experimental analysis of transmission line parameters in high-speed GaAs digital circuit interconnects. *IEEE Transactions on Microwave Theory and Techniques*, 1991, 39(8): 1361–1367
 44. Colin R E. *Foundation for Microwave Engineering*. 2nd ed. Hoboken: John Wiley & Sons, 2007
 45. Yao X S, Maleki L. High frequency optical subcarrier generator. *Electronics Letters*, 1994, 30(18): 1525–1526
 46. Zhang H, Pan S, Huang M, Chen X. Polarization-modulated analog photonic link with compensation of the dispersion-induced power fading. *Optics Letters*, 2012, 37(5): 866–868
 47. Pan S, Yao J. A frequency-doubling optoelectronic oscillator using a polarization modulator. *IEEE Photonics Technology Letters*, 2009, 21(13): 929–931
 48. Pan S, Yao J. Tunable subterahertz wave generation based on photonic sextupling using a polarization modulator and a wavelength fixed notch filter. *IEEE Transactions on Microwave Theory and Techniques*, 2000, 58(7): 1967–1975
 49. Zhu D, Pan S, Ben D. Tunable frequency-quadrupling dual-loop optoelectronic oscillator. *IEEE Photonics Technology Letters*, 2012, 24(3): 194–196
 50. Zhu D, Liu S, Pan S. Multichannel up-conversion based on polarization –modulated optoelectronic oscillator. *IEEE Photonics Technology Letters*, 2014, 26(6): 544–547
 51. Zhu D, Pan S, Cai S, Ben D. High-performance photonic microwave downconverter based on a frequency-doubling optoelectronic oscillator. *Journal of Lightwave Technology*, 2012, 30(18): 3036–3042
 52. Tang Z, Pan S. Transmission of 3-Gb/s uncompressed HD video in an optoelectronic-oscillator-based radio over fiber link. In: *Proceeding of Radio and Wireless Symposium, Austin, IEEE*, 2013, 319–321
 53. Li W, Zhang W, Yao J. Frequency-hopping microwave waveform generation based on a frequency-tunable optoelectronic oscillator. In: *Proceeding of Optical Fiber Communications Conference and Exhibition (OFC), San Francisco, IEEE*, 2014, 1–3
 54. Jiang Z, Huang C B, Leaird D E, Weiner A M. Optical arbitrary waveform processing of more than 100 spectral comb lines. *Nature Photonics*, 2007, 1(8): 463–467
 55. Chen C, Zhang F, Pan S. Generation of seven-line optical frequency comb based on a single polarization modulator. *IEEE Photonics Technology Letters*, 2013, 25(22): 2164–2166
 56. Li W, Wang W T, Sun W H, Wang L X, Liu J G, Zhu N H. Generation of flat optical frequency comb using a single polarization modulator and a Brillouin-assisted power equalizer. *IEEE Photonics Journal*, 2014, 6(2): 1–8
 57. He C, Pan S, Guo R, Zhao Y, Pan M. Ultraflat optical frequency comb generated based on cascaded polarization modulators. *Optics Letters*, 2012, 37(18): 3834–3836
 58. Wang M, Yao J. Tunable optical frequency comb generation based on an optoelectronic oscillator. *IEEE Photonics Technology Letters*, 2013, 25(21): 2035–2038
 59. Tang Z, Pan S, Zhu D, Guo R, Zhao Y, Pan M, Ben D, Yao J. Tunable optoelectronic oscillator based on a polarization modulator and a chirped FBG. *IEEE Photonics Technology Letters*, 2012, 24(17): 1487–1489
 60. Zhang Y, Pan S. Complex coefficient microwave photonic filter using a polarization-modulator-based phase shifter. *IEEE Photonics Technology Letters*, 2013, 25(2): 187–189
 61. Zhang Y, Wu H, Zhu D, Pan S. An optically controlled phased array antenna based on single sideband polarization modulation. *Optics Express*, 2014, 22(4): 3761–3765



Yu Xiang received the B.S. degree in optical engineering from Zhejiang University, Hangzhou, China, in 2006, and the M.S. degree in photonics from Royal Institute of Technology (KTH), Stockholm, Sweden, in 2008. He received the Ph.D. degree in applied physics from KTH in 2014, working on design and fabrication of GaAs-based vertical-cavity surface-emitting transistor-lasers (T-VCS

ELs).

In 2015, he joined the Key Laboratory of Radar Imaging and Microwave Photonics (Nanjing University of Aeronautics and Astronautics), Ministry of Education. Currently, he is a lecturer in Electronic and Information Engineering with research interests in the development of GaAs-based integrated optoelectronic devices and circuits for microwave photonics applications.



Shilong Pan received the B.S. and Ph.D. degrees in electronics engineering from Tsinghua University, Beijing, China, in 2004 and 2008, respectively. From 2008 to 2010, he was a “Vision 2010” Postdoctoral Research Fellow in the Microwave Photonics Research Laboratory, University of Ottawa, Canada. He joined the College of Electronic and Information Engineering, Nanjing University of Aeronautics and Astronautics (Nanjing Univ. Aeronaut. Astronaut.), China, in 2010, where he is currently a full professor and executive director of the Key Laboratory of Radar Imaging and

Microwave Photonics (Nanjing Univ. Aeronaut. Astronaut.), Ministry of Education.

His research has focused on microwave photonics, which includes optical generation and processing of microwave signals, ultrawide-band over fiber, photonic microwave measurement, and integrated microwave photonics. Prof. Pan has authored or co-authored over 230 research papers, including more than 120 papers in peer-reviewed journals and 110 papers in conference proceedings.

Prof. Pan is a senior member of the IEEE Microwave Theory and Techniques Society, the IEEE Photonics Society and a member of the Optical Society of America (OSA). He was selected to receive an OSA outstanding reviewer award in 2015. Prof. Pan is a Chair of numerous international conferences and workshops, including the TPC Chair of the International Conference on Optical Communications and Networks in 2015, TPC Chair of the high-speed and broadband wireless technologies subcommittee of the IEEE Radio Wireless Symposium in 2013, 2014 and 2016, TPC Chair of the Optical fiber sensors and microwave photonics subcommittee chair of the OptoElectronics and Communication Conference in 2015, and Chair of the microwave photonics for broadband measurement workshop of International Microwave Symposium in 2015.